Morphometric Variation at Different Spatial Scales: Coordination and Compensation in the Emergence of Organismal Form

Philipp Mitteroecker[1,2,*], Silvester Bartsch[1], Corinna Erkinger[1], Nicole D. S. Grunstra[1,2,3], Anne Le Maître[1,4,5] and Fred L. Bookstein[1,6]

[1]*Department of Evolutionary Biology, University of Vienna, Vienna, Austria;* [2]*KLI Institute for Evolution and Cognition Research, Klosterneuburg, Austria;* [3]*Mammal Collection, Natural History Museum Vienna, Vienna, Austria;* [4]*Laboratoire Paléontologie Evolution Paléoécosystèmes Paléoprimatologie (PALEVOPRIM) - UMR 7262 CNRS INEE, Université de Poitiers, Poitiers, France;* [5]*Department of Palaeontology, University of Vienna, Vienna, Austria; and* [6]*Department of Statistics, University of Washington, Seattle, WA, USA*
*Correspondence to be sent to: Althanstrasse 14, A-1090 Vienna, Austria; E-mail: philipp.mitteroecker@univie.ac.at.

Abstract.—It is a classic aim of quantitative and evolutionary biology to infer genetic architecture and potential evolutionary responses to selection from the variance–covariance structure of measured traits. But a meaningful genetic or developmental interpretation of raw covariances is difficult, and classic concepts of morphological integration do not directly apply to modern morphometric data. Here, we present a new morphometric strategy based on the comparison of morphological variation across different spatial scales. If anatomical elements vary completely independently, then their variance accumulates at larger scales or for structures composed of multiple elements: morphological variance would be a power function of spatial scale. Deviations from this pattern of "variational self-similarity" (serving as a null model of completely uncoordinated growth) indicate genetic or developmental coregulation of anatomical components. We present biometric strategies and R scripts for identifying patterns of coordination and compensation in the size and shape of composite anatomical structures. In an application to human cranial variation, we found that coordinated variation and positive correlations are prevalent for the size of cranial components, whereas their shape was dominated by compensatory variation, leading to strong canalization of cranial shape at larger scales. We propose that mechanically induced bone formation and remodeling are key mechanisms underlying compensatory variation in cranial shape. Such epigenetic coordination and compensation of growth are indispensable for stable, canalized development and may also foster the evolvability of complex anatomical structures by preserving spatial and functional integrity during genetic responses to selection.[Cranial shape; developmental canalization; evolvability; morphological integration; morphometrics; phenotypic variation; self-similarity.]

"The problem of individuality is merely an expression of the fact that you do have a greater constancy at the higher level of the organized individual system than you have of its constituent parts. That is, identical twins are much more similar than are any microscopic sections from corresponding sites you can lay through either of them."
Paul Weiss, 1956 (as quoted by Gerard, 1958, p. 140)

The coordinated development of complex anatomical structures, such as the vertebrate cranium, requires the integrated growth of spatially and functionally related traits. At a mechanistic level, such a coordination of individual development can arise from mechanical interactions and chemical signaling across developing tissues or from growth factors with systemic effects. At the population level, integrated variation of otherwise independent elements can result from the evolutionary fine-tuning of pleiotropic gene effects (Cheverud 1982, 1984; Zelditch et al. 2006; Hallgrimsson et al. 2007b; Mitteroecker et al. 2012; Pavlicev and Wagner 2012; Armbruster et al. 2014; Hall 2015; Hallgrímsson et al. 2019). Some of these genetic and developmental factors may have similarly directed effects on related structures, causing coordinated variation. For instance, long upper jaws co-occur with long lower jaws, and vice versa, thus enabling proper occlusion of teeth and effective mastication. For other structures, compensatory growth processes may result in covariation in opposite directions. For example, to achieve a properly sized upper jaw, a relatively short premaxilla may be compensated by a longer maxilla, and a relatively long premaxilla by a shorter maxilla. This compensatory variation at the level of components (maxillary and premaxillary bones) leads to reduced variation—*canalization*—at the larger scale (upper jaw), thus stabilizing the development of functionally relevant units. Without compensatory growth variance accumulates across components, leading to an increase of variance with spatial scale.

Even though both growth patterns, coordination and compensation, are prerequisites of stable individual development and integrated evolution, they are usually lumped under the term "morphological integration" in the morphometric and evolutionary literature. Most studies in the Olson and Miller (1958) tradition have interpreted a correlation of zero between traits as evidence for genetic and developmental independence. This interpretation is not warranted for many kinds of measurements, particularly not for measurement *point*s ("landmarks"). Even if different anatomical components should lack any common control, nearby measurement points would still be correlated simply because of their spatial adjacency (Mitteroecker and Bookstein 2007; Mitteroecker et al. 2012; Bookstein 2015; Gonzalez et al. 2019). However, a complete lack of coregulation would manifest at another level: If all parts vary completely independently, then their size variance accumulates at larger scales; morphological variation would be a function of the spatial scale at which it is studied. *But if appropriately corrected for*

scale, the variational properties would be the same across different spatial scales or across structures of different sizes (see the following sections for specific models). In probability theory and signal processing, this property is referred to as variational "self-similarity" (e.g., Mandelbrot and Van Ness 1968; Leland et al. 1994; Embrechts and Maejima 2002; Mardia et al. 2006). In morphometrics, deviations from this pattern of self-similar variation would indicate the action of coordinating or compensatory growth processes (manifested by an excess or deficiency of variation at larger scales, respectively).

Formally, an intrinsic random process $\{X(t), t \geq 0\}$ or random field (a spatial random process in d dimensions) $\{X(t), t \in \mathbb{R}^d\}$ is said to be self-similar if there exists $\alpha > 0$ such that the process or field $\{c^{-\alpha} X(ct)\}$ has the same distribution as $\{X(t)\}$ for any $c > 0$. In other words, for a random self-similar process, the variable X, observed once over a small temporal or spatial scale t, and once over a larger scale ct, has the same variance, σ^2, if appropriately corrected by a power function of the ratio in scale, c:

$$\sigma^2_{X(t)} = \frac{\sigma^2_{X(ct)}}{c^{2\alpha}}. \qquad (1)$$

(e.g., Embrechts and Maejima 2002). The index α is referred to as the self-similarity index; it is multiplied by 2 because the formula refers to the variance (squared unit). Deviations from this pattern of variational self-similarity indicate nonzero correlation between temporal or spatial increments, or in the present context, some coregulation of the constituting anatomical parts: coordination, compensation, or a combination of both.

Morphological variation at different spatial scales is subject to different selective pressures and evolutionary processes. For instance, the overall length of the upper jaw in vertebrate animals is of functional relevance for mastication and thus subject to natural selection. As a result, parallel or convergent evolution in different species is likely to lead to homoplasies in jaw length (Wake 1991; Hodin 2000), regardless of the relative contributions of premaxilla, maxilla, and palatine to upper jaw length, which are of less functional relevance. Compensatory variation of these small-scale features may largely be selectively neutral and more abundant than variation of functional traits within a population. Hence, *across* populations, compensatory variation of small-scale features may largely be subject to evolutionary drift and convey a more reliable phylogenetic signal than the functionally relevant large-scale features. Morphometric studies of adaptive evolution and phylogenetic history would thus profit from a separation of large-scale from small-scale aspects of organismal from. Contrasting morphological variation across different spatial scales would also help to identify morphological loci of stabilizing selection and developmental canalization.

In this article, we present models of variational self-similarity and the corresponding scaling factor, α, for two kinds of morphometric measurements: extensive measures (i.e., measurements that add up) of length and area, and intensive measures of the shape of landmark configurations. From these models, we derive biometric strategies for studying morphological variation at different spatial scales and for identifying patterns of coordination and compensation. We apply these methods to size and shape variation of human crania and provide R scripts (R Core Team 2019).

A Model for Extensive Size Measurements

Consider, first, a structure composed of two parts, each of which can be represented by an extensive size measure such as length, area, or volume. If the total size, S, of the structure equals the sum of the sizes of its two parts, $S = A + B$, then the sample average of total size is given by the summed averages of the two parts, and the sample variance of total size can be decomposed into the variances of its components plus twice their covariance:

$$\mathrm{Var}(S) = \mathrm{Var}(A) + \mathrm{Var}(B) + 2\mathrm{Cov}(A, B). \qquad (2)$$

Depending on the correlation between A and B, three cases can be distinguished in this toy model:

1. The sizes of A and B are uncorrelated, as it may occur—hypothetically—under completely independent developmental control. In this case, the variances of the parts add up to the variance of the whole as the covariance term in equation 2 vanishes: $\mathrm{Var}(A + B) = \mathrm{Var}(A) + \mathrm{Var}(B)$. We refer to this case as *nonregulation* because the two parts vary completely independently, without common regulation.

2. A and B are positively correlated, which we refer to as *coordinated variation*. As a result, total size is more variable than the summed variances of its parts: $\mathrm{Var}(A + B) > \mathrm{Var}(A) + \mathrm{Var}(B)$.

3. A and B are negatively correlated due to *compensatory variation*. In this case, the variance of total size is smaller—more canalized—than the summed variances of its parts because the covariance term in equation 2 is negative: $\mathrm{Var}(A + B) < \mathrm{Var}(A) + \mathrm{Var}(B)$.

The case of nonregulation separates the two opposite scenarios of coordination versus compensation. In practice, nonregulated variation rarely results from completely independent developmental control but from a balance between coordinating and compensating processes, that is, from the canceling of genetic or developmental factors inducing positive and negative correlations (Cheverud 1984; Mitteroecker and Bookstein 2007; Mitteroecker 2009; Pavlicev and Wagner 2012). Positive net correlations indicate the dominance of coordinating over compensating processes, and *vice versa* for negative net correlations.
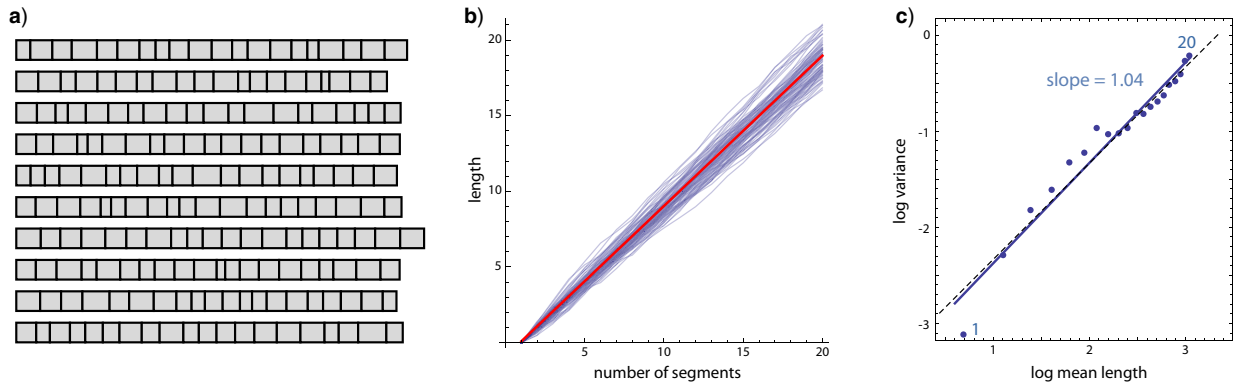
FIGURE 1. a) Ten random instances of a "one-dimensional" anatomical structure, each one consisting of 20 differently sized segments. Here, these segments vary completely independently in length, drawn from a normal distribution with mean 1.0 and variance 0.04. b) For a sample of 100 such structures, the cumulative length of the segments is plotted against segment number. Each of the resulting curves is equivalent to a *random walk*, a stochastic increment process in which each step is independent of its current state. Because the segments vary independently, both their means and variances add up; the expected variance of total length is a linear function of the number of segments. c) For increasing segment number, the variance in length is plotted against mean length across the 100 random structures. The regression slope in this log–log plot is 1.04, close to the expected value of 1 for a linear relationship, one in which both mean and variance relates linearly to the number of elements.

These considerations extend to structures composed of multiple parts with sizes P_i, enumerated from $i = 1$ to n. Average total size can be expressed as the sum of all the part's averages,

$$\bar{S} = \sum_{i=1}^{n} \bar{P}_i,$$

and the variance of total size equals the summed variances of the parts plus all pairwise covariances:

$$\text{Var}(S) = \sum_{i=1}^{n} \text{Var}(P_i) + \sum_{i \neq j}^{n,n} \text{Cov}(P_i, P_j).$$

Again, if all parts were mutually uncorrelated, their variances would add up, just like their means. This implies that for parts with homogeneous means and variances, the variance of a composite structure would scale linearly with its mean size: both are a function of the number of parts, n.

Figure 1 illustrates this for simple "one-dimensional" structures, such as a cross-sectional sample of segmented worms. The length of each segment is drawn randomly from a normal distribution with $\mu = 1$ and $\sigma = 0.2$. Hence, all segments have the same mean and variance, and they all vary independently: they behave in a completely nonregulated or uncoordinated way. For increasing numbers of segments, Figure 1b plots total worm length against segment number, illustrating how both the mean and the variance of total length increase linearly with the number of segments included. The regression of total length on segment number has an expected slope of 1, the mean segment length, μ. The expected slope of the variance of total length on segment number is 0.04, the variance of segment length, σ^2. Hence, also mean and variance of total length scale linearly, leading to a slope of 1 and an intercept of $\log \sigma^2$ on a log–log scale (Fig. 1c).

The linear relationship between mean and variance for differently sized substructures in the case of nonregulation resembles the well-known properties of a random walk with linear drift: a random process $\{X(t)\}$ with independent and identically normally distributed increments (the discrete version of a Wiener process or Brownian motion). For such a process, both the variance and the mean of $X(t)$ are linear functions of the number of increments, t. Also, the covariance between $X(t)$ and $X(s)$ is just a function of the lag or "distance" $|s - t|$ (this property characterizes an "intrinsic" random process).

In such a system, the variance of a substructure *relative* to its average size—the *scale-corrected variance* $\sigma_c^2 = \text{Var}(S)/\bar{S}$—would be constant across differently sized structures, consistent with the definition of self-similarity if $\alpha = \frac{1}{2}$ (equation 1). (Note that this statistic differs from the more commonly used coefficient of variation, which expresses the standard deviation, not the variance, as a fraction of the mean.) An anatomical structure with this self-similar property would vary in a completely uncoordinated way; every part is growing independently of all others, without any common control. Clearly, this behavior does not reflect the well-coordinated ontogeny of 3D tissues and organs in multicellular organisms. But it serves as a null model in-between the two alternatives of coordinated versus compensatory growth.

If the parts of an organism grow in a coordinated way (Fig. 2a–c), leading to positive correlations among parts, the variance of total size increases faster than linearly with mean size, and the slope of log variance on log mean size is larger than 1. Hence, also the scale-corrected variance increases with the average size of the structure. By contrast, if compensatory processes dominate over coordinated ones, correlations among parts tend to be negative, and the scale-corrected variance decreases with scale: the larger the structure,
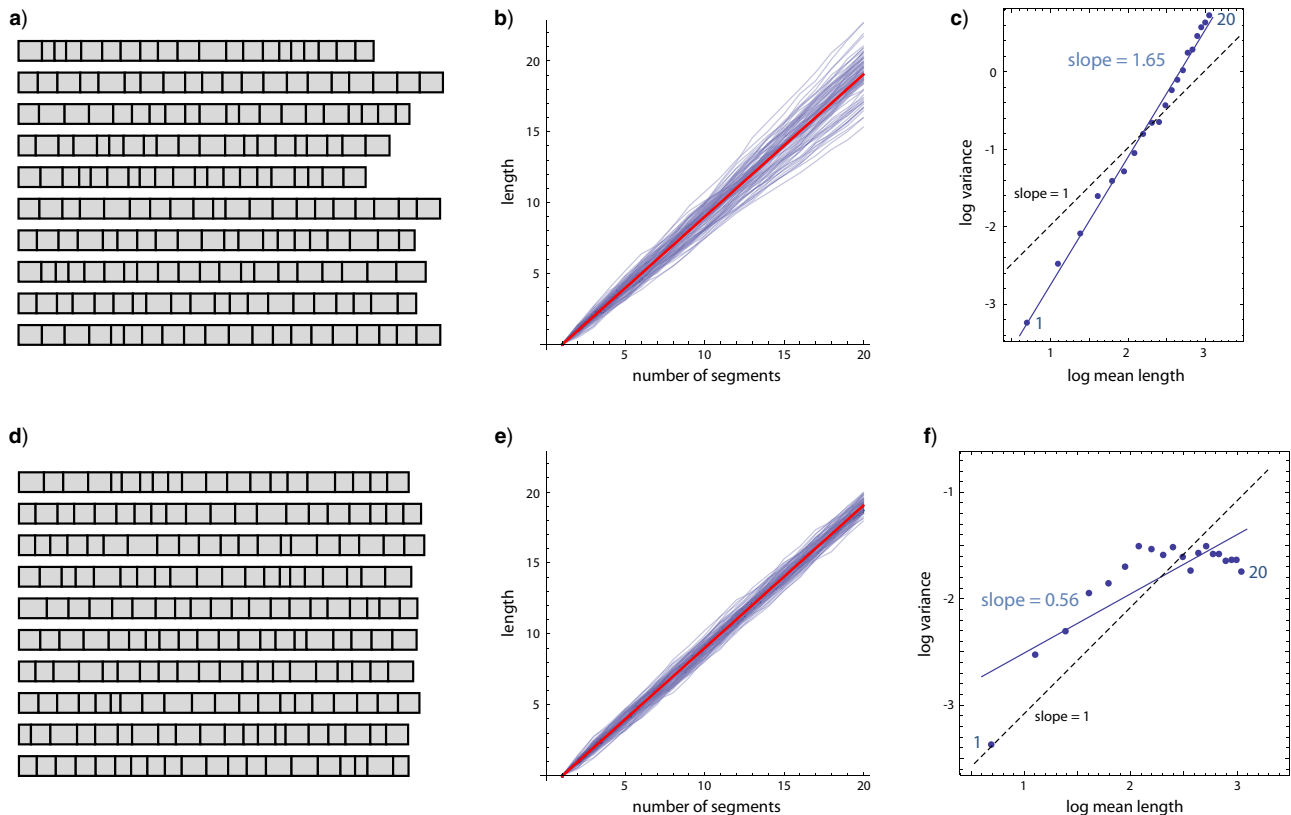
FIGURE 2.   a) Another 10 instances of a segmented structure as in Figure 1, but here the segments are not independent, they show positive correlations instead. In other words, the segments show a certain degree of *coordination* in length. In comparison with Figure 1a, the total length of these structures is more variable, which is also apparent in (b): the variance increases faster than linearly with the number of segments. c) As a result, the regression slope of log variance on log mean length is larger than 1. d) Here the segments show negative correlations, reflecting a *compensation* in length. Total length thus is less variable than in Figure 1. e, f) Variance in length increases with mean length only for the first few elements and then levels off, leading to a slope of less than 1 in the log–log plot.

the more it is canalized (the slope of log variance on log mean size is smaller than 1; Fig. 2d–f). The corresponding compensatory curves in Figure 2e are autoregressive processes of order 1 (here with a mean-reversion rate of 0.07), the discrete version of an Ornstein–Uhlenbeck process (a mean-reverting continuous-time stochastic process). Note that an autoregressive process has a stationary variance, that is, after a certain number of increments (seven in this example) the expected variance stays constant.

This model of self-similarity can be applied to study linearly extending segmented anatomical structures, such as the vertebral column, tooth rows, or limbs as well as to simple segmented organisms, such as annelids. But the model can also be applied to measures of area, volume, or mass of more complex structures or organisms, as in the empirical example below. Self-similar variation of area or volume with $\alpha = \frac{1}{2}$ (linear relationship between mean and variance) would result from an aggregation of independently varying elements without apparent geometric constraints, or from the independent variation of loosely connected organs (so that they *could* vary independently without any constraints owing to shared boundaries).

In empirical studies of structures that can be decomposed exhaustively into nonoverlapping parts, a cross-sectional variance of total size exceeding the summed variances of the parts indicates an excess of coordinating processes over compensating ones, and *vice versa* for a lower variance of total size. For overlapping parts or nonexhaustive partitionings, scale-corrected variances can still be compared among differently sized parts, and log-transformed variances can be regressed on log mean sizes. Slopes larger or smaller than 1 indicate a dominance of coordinated or compensatory variation, respectively. The intercept is determined by the average variance per size unit (and measurement error, see below). Similar approaches, including such log–log plots, have a long tradition in signal processing (e.g., Hurst 1951; Leland et al. 1994; Cannon et al. 1997).

A MODEL FOR SHAPE

In addition to size variation, shape variation among landmark configurations can be decomposed into different spatial scales, but such analyses are limited to the nonaffine (i.e., local) aspects of shape variation. Affine transformations are linear transformations (linear scaling and shearing); they are the same at all locations
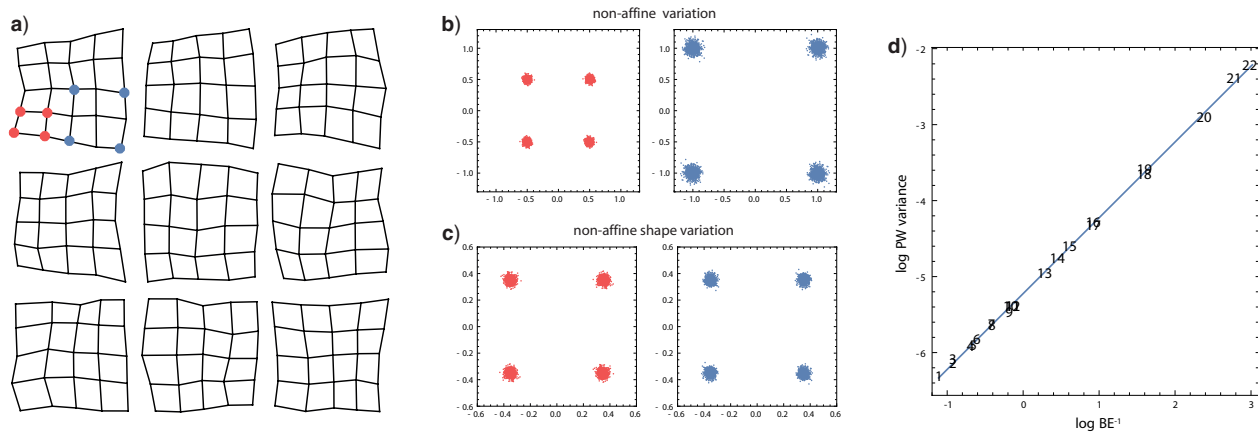
FIGURE 3.   Self-similar variation of a 5×5 grid of landmarks. a) Nine landmark configurations showing random self-similar variation around a regular square grid (for formulas see Supplementary material available on Dryad). b) Nonaffine "Boas" coordinates (nonaffine shape coordinates rescaled to their original size) of the lower left four landmarks (red points, left panel) and the lower right four landmarks (blue points, right panel) for 1000 such random grids. The blue landmark configurations are, on average, twice as large as the red landmark configurations, and the nonaffine landmark variation is four times as large as that of the red landmarks. c) When scaled to the same size, the small and the large configurations show the same amount of nonaffine shape variance. d) The 22 PWs of these 25 landmarks are shape features with increasing spatial scale (specified by inverse bending energy, BE^{-1}, as a measure of squared scale). For self-similar variation, the variance of these PWs increases linearly with inverse BE, leading to a slope of 1 in the regression of log variance on log BE^{-1}.

and also at all spatial scales (their spatial scale is infinite; Bookstein 1991; Rohlf and Bookstein 2003). Only nonlinear shape transformations can be localized and thus show a finite spatial scale; these are the nonaffine transformations (see Supplementary Fig. S1 available on Dryad at http://dx.doi.org/10.5061/dryad.j6q573n8s). The comparison of shape variation across different spatial scales thus is inherently limited to the nonaffine component of shape variation (Bookstein 2015).

For the size measures in Figure 1, the one-dimensional random walk gave rise to a linear relationship between the variance and the number of elements ("scale"); the scale-corrected variance was the same at all scales. Figure 3 shows the analog of a 1D random walk for 2D shape: a self-similar distribution of landmark variation (see Bookstein 2015 or Supplementary material available on Dryad for computational details). The configurations in Figure 3a consist of 25 landmarks each, arranged as the vertices of 5×5 grids. Like the increments of a random walk, every grid cell has the same nonaffine shape distribution, and the variance of larger grid elements composed of multiple grid cells (larger squares with corners on the grid) is a linear function of the number of cells (area or squared scale). Note that we refer here to the variance (summed over all landmark coordinates) after removing the affine term and standardizing the configurations for location and orientation, but not scale (referred to as "Boas coordinates" in Bookstein 2018). *After* correcting for scale, the magnitude of nonaffine shape variation is the same at all scales.

For instance, the area of the polygon spanned by the blue landmarks (delineating a 2×2 grid) is, on average, four times as large as that of the red landmarks (delineating a 1×1 grid), and also the nonaffine Boas variance of the blue landmarks is four times that of the red landmarks (Fig. 3b). After scaling them all to the

same size, they show the same amount of nonaffine shape variance (Fig. 3c), just like the scale-corrected variance of a random walk. These relationships apply as well to every other square landmark configuration, such as one at 45° to the grid.

Under a model of self-similar landmark variation, the linear association between squared scale and nonaffine Boas variance holds only for configurations with the same mean shape, such as the four vertices of the grid cells. But self-similarity of shape variation can also be studied by exploiting the self-similar property of the thin-plate spline interpolation (Kent and Mardia 1994; Mardia et al. 2006; Bookstein 2015). Nonaffine shape variation (with $2k-6$ degrees of freedom for k 2D landmarks) can be decomposed into an orthogonal set of shape features with increasing spatial scale, the *principal warps* (Bookstein 1989, 1991). Computationally, the principal warps are the $k-3$ eigenvectors of the bending energy (BE) matrix (see Supplementary material available on Dryad) and are each associated with a *bending energy* (the corresponding eigenvalue), which is an inverse measure of squared spatial scale. Large BEs correspond to principal warps that describe small-scale features (deformations of landmarks that are close together), while a small BE characterizes a large-scale deformation. Affine deformations have zero BE because they are of infinite spatial scale (see Supplementary Fig. S1 available on Dryad).

When expressing shape variation within a sample in terms of these successive deformations, each principal warp applies twice, once to the x-coordinates and once to the y-coordinates; the corresponding partial deformations are called *partial warps* (PWs). The $2(k-3)$ PW *scores* are the orthogonal projections of the shape vectors on the principal warp vectors, separately for x and y. In other words, PW scores describe
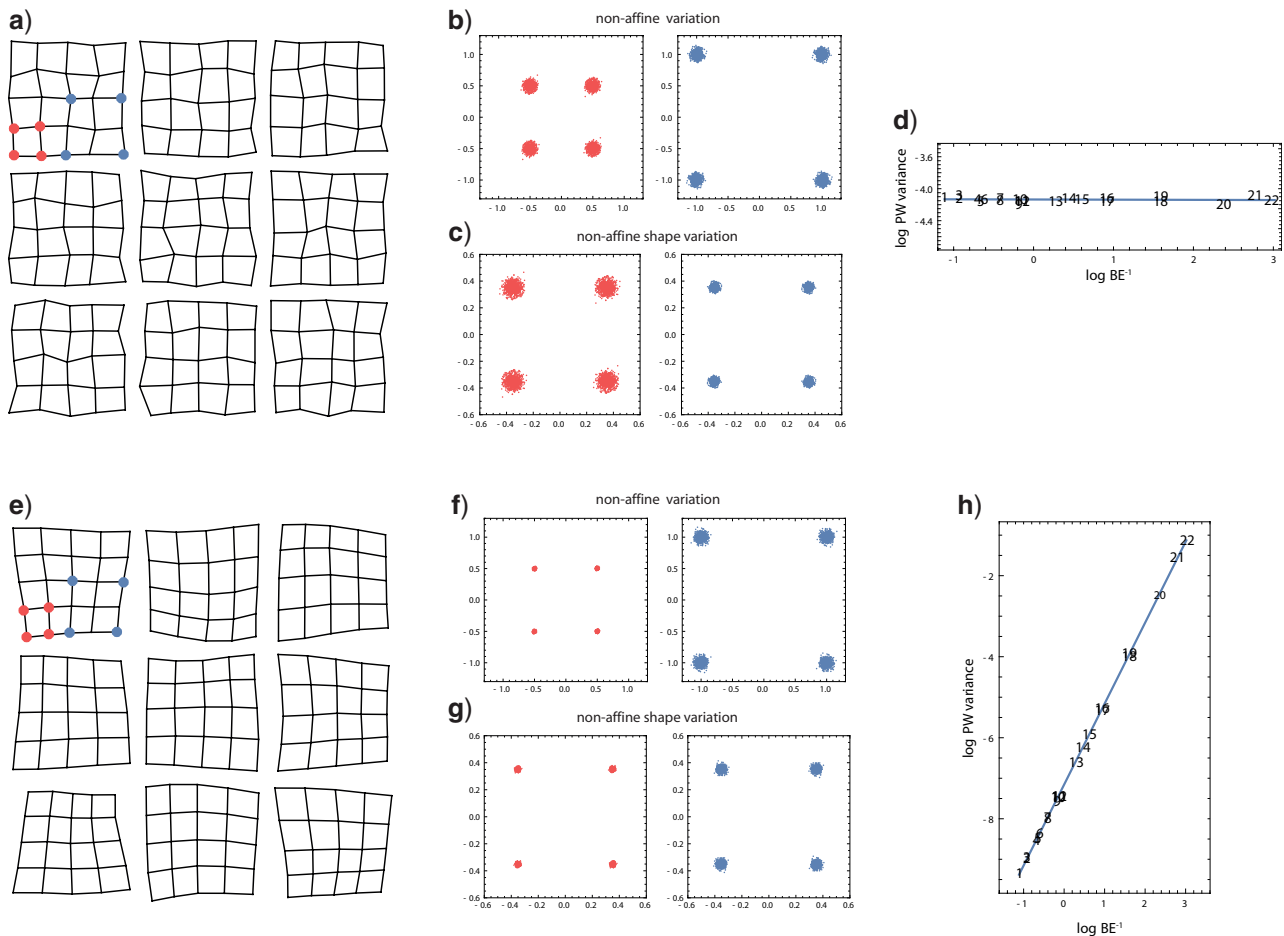
FIGURE 4. Examples of compensatory (top) and coordinated (bottom) landmark variation. a) Nine configurations showing compensatory variation. b) Here, nonaffine Boas variance does not increase with spatial scale; it is the same for squares of size 1 (red, left panel) and squares of size 2 (blue, right panel). c) When scaled to the same size, nonaffine shape variance decreases with scale, that is, large structures show less shape variance than small structures. d) The variance of the PWs is the same for all spatial scales. e) Nine configurations showing coordinated variation. f) Here, nonaffine Boas variance increases steeply with spatial scale; the variance of squares of size 1 (red) is less than one-quarter of the variance of squares of size two (blue). g) Even nonaffine shape variance increases with spatial scale. h) As a result, the variance of PWs increases faster than linearly with scale (a slope of 2 in the log-log plot).

nonaffine shape variation in terms of shape features with different spatial scales (rather than in terms of the shapes of differently sized substructures). For a self-similar variance pattern, the variance of PW scores scales linearly with inverse BE (as a measure of squared scale), that is, they show a slope of 1 in a log–log plot (Fig. 3d).[1] In that case, relative to scale, every PW shows the same variance.

Figure 4a–d shows another set of 5×5 landmark grids, but here variation is compensatory, not self-similar: nonaffine Boas variance increases less than linearly with spatial scale. Corrected for scale, shape variance decreases with scale (Bookstein 2015 referred

to this as "disintegrated" shape variation). The opposite scenario is depicted by Figure 4e–h: the landmarks vary in a coordinated way (see the Supplementary material available on Dryad for computational details). As a result, nonaffine Boas variance increases faster than linearly with squared scale (Fig. 4f,h); corrected for scale, nonaffine shape variance increases with scale (Fig. 4g).

The linear relationship between nonaffine variance and squared spatial scale that characterizes self-similar landmark variation (with $\alpha=1$) can serve as reference in empirical morphometric studies. In a log–log plot of the cross-sectional sample variance against inverse BE for each PW, a slope >1 indicates an excess of coordinated variation, whereas a slope <1 would result from a dominance of compensatory variation. Note, however, that the models of self-similar size and shape variation from which these statistics derive resemble a homogenous tissue with isotropic variational properties of all elements (i.e., all the

---

[1]Note that the horizontal axis in this and the following two figures differ from the presentations in Bookstein (2015, 2017, 2018), where this axis shows log BE, representing inverse scale, not the negative of that logarithm. An increase along this axis thus corresponds to an increase (not a decrease) in spatial scale, and the orientation of the corresponding regression line matches that of the self-similar size process in Figure 1.
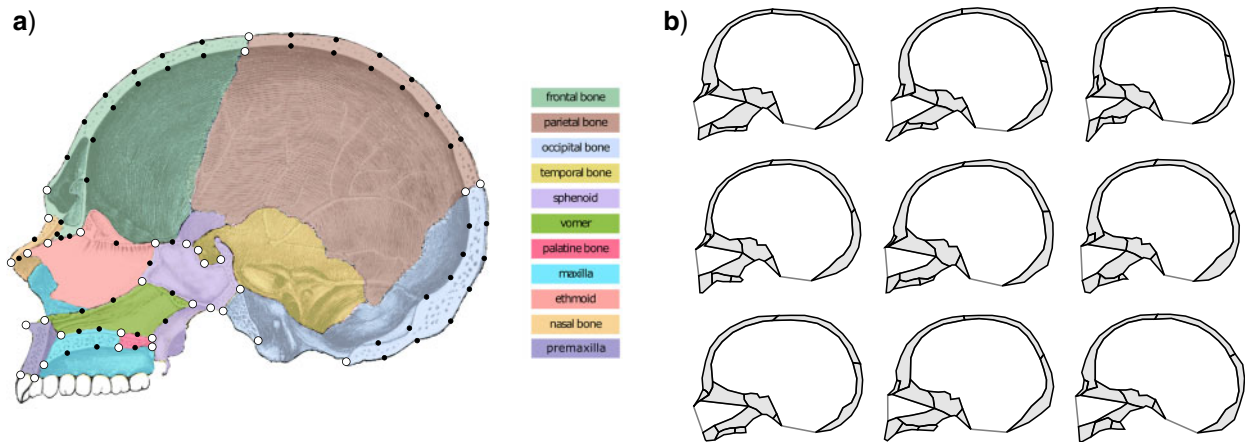
FIGURE 5.   a) Midsagittal landmarks digitized on high-resolution CT scans of a geographically diverse sample of 24 adult human crania (16 females, 8 males). The different bones are shown in separate colors (modified from Gray 1918). A set of 32 3D anatomical landmarks (white dots) and 55 semilandmarks (black dots) were measured on every CT scan using Avizo (Thermo Fisher Scientific) and then projected onto a least-squares-fitted plane. The positions of the semilandmarks along their curves were estimated by the sliding landmark algorithm, which slides the semilandmarks along the curves in order to minimize the total BE, a measure of local shape difference, between each specimen and the sample average (Bookstein 1997; Gunz and Mitteroecker 2013). b) The cross-sectional areas of the different cranial bones, the nasal cavity, the braincase, and the entire cranial cross-section were approximated by polygons defined by the measured landmarks, as exemplified here for nine arbitrary individuals of the sample.

differently sized substructures are composed of different numbers of elements with homogenous mean and variance properties). Most real anatomical structures deviate from this model. Depending on the structural heterogeneity encountered, only substantial departures from self-similarity should be interpreted as evidence for compensating or coordinating processes. Deviations of single size or shape factors from an otherwise homogeneous variational pattern may require separate interpretation (Bookstein 2017).

EXAMPLE: HUMAN CRANIAL FORM

We analyzed size and shape variation within a sample of 24 adult human crania. Using high-resolution CT scans, we measured 87 2D landmarks and semilandmarks (Bookstein 1991; Gunz and Mitteroecker 2013) on each specimen to delineate the midsagittal outlines of all the cranial bones and cavities (for details see Fig. 5 and Bartsch 2019). From these landmarks, we completely partitioned the cranial midsection (the area within the cranial outline) into the cross-sectional areas of the cranial bones, the braincase, and the nasal cavity (Fig. 5b). As the occipital bone is separated in the midplane by the foramen magnum, we treated the basilar and posterior parts of the occipital as two separate structures.

We calculated mean and variance for the area of each cranial element. The variance of the entire midsection (2.22×10^6 mm^4) clearly exceeded the sum of the variances of the cranial parts (1.17×10^6 mm^4), and the regression slope of log variance on log mean was 1.49 (Fig. 6a), indicating a faster than linear increase of variance with mean size and a dominance of coordinated variation. The scale-corrected variances of the cranial

parts differed considerably: larger structures were more variable *relative* to their scale than smaller structures (Fig. 6b).

Figure 7 shows the correlation matrix for the midsagittal areas of the cranial bones and its first two principal components (PCs). Indeed, positive correlations are prevailing, especially among neurocranial bones and among facial bones. The basilar part of the occipital stands out as the least correlated bone. PC 1 loads positively on all variables, except the basioccipital, and represents a common size factor that accounts for most of the coordination (positive correlations) among cranial parts. The second PC loads positively on the neurocranial bones and negatively on facial bones, thus accounting for the weak negative correlations between some of the facial and neurocranial bones. Hence, despite the overall dominance of coordinated variation in the size of cranial bones, facial and neurocranial size also show some compensatory variation.

We also studied the midsagittal shapes of the cranial bones and cavities, as captured by the 2D landmarks. In contrast to area, the cross-sectional shape of larger structures varied considerably less than the shape of smaller structures (Fig. 8, left). For a self-similar pattern of shape variation, nonaffine shape variance would be the same at every scale, but nonaffine shape variance of the cranial elements clearly decreased with squared centroid size (as a measure of squared scale; Fig. 9a).[2]

---

[2]Note that in order to compare shape variation across configurations with different numbers of landmarks, k, centroid size needs to be divided through $\sqrt{k}$, and also total variance (summed variances of all shape coordinates) must be divided through k. Combined, however, these two corrections cancel and can be omitted (because the
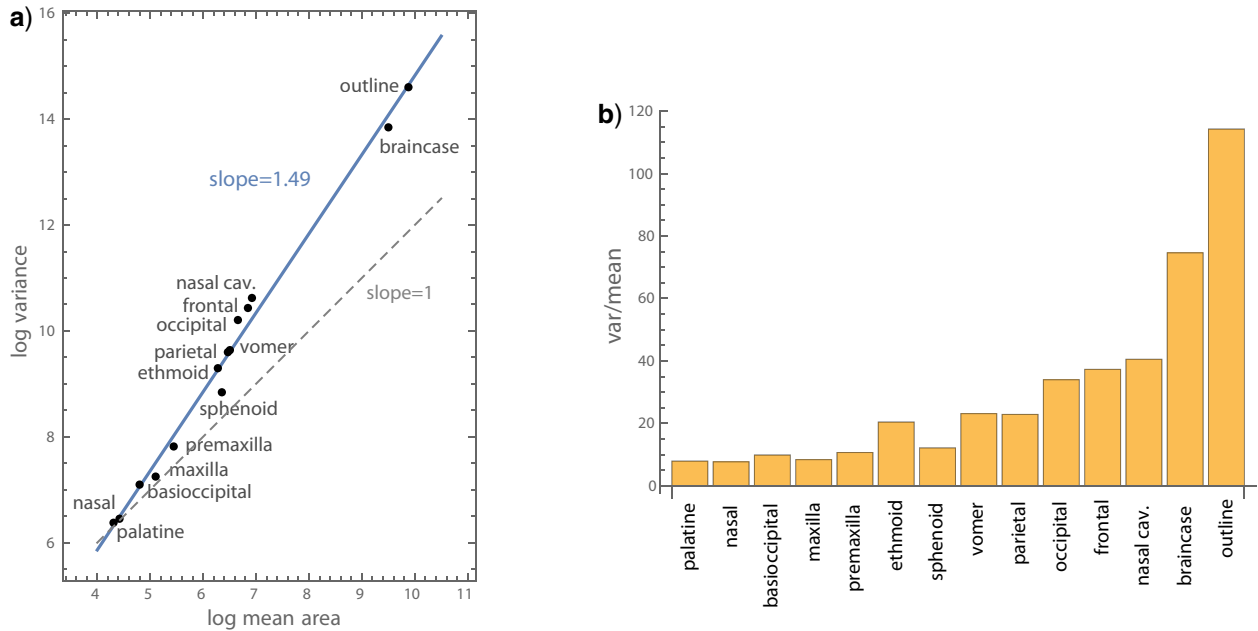
FIGURE 6.   a) Plot of sample variance versus mean for the cross-sectional areas of the cranial structures. On this log–log scale, the linear regression (blue line) has a slope of 1.49, clearly above 1 (dashed line). b) For each of the cranial structures (ordered from the smallest to the largest), the variance of the cross-sectional area divided by the mean area ("scale-corrected variance") is plotted.
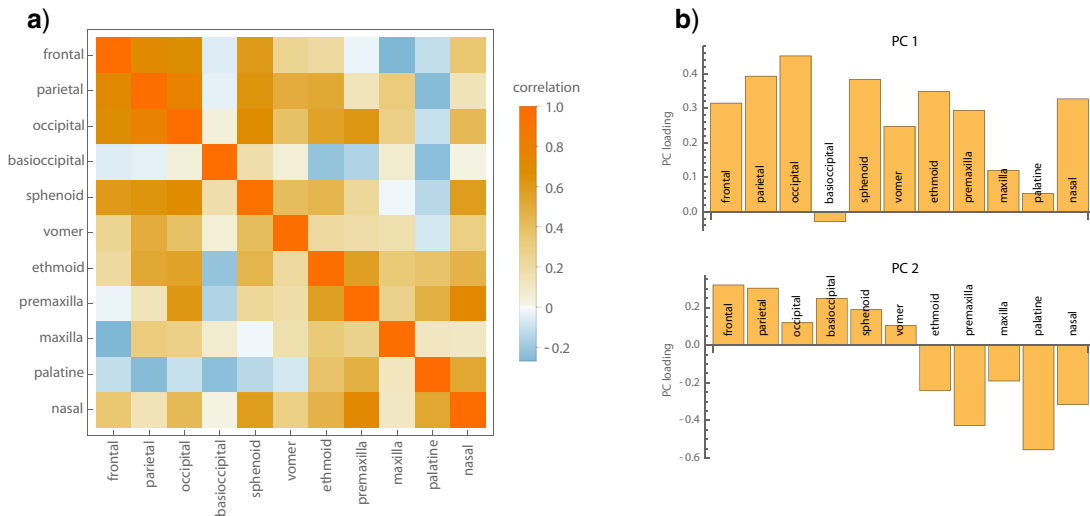

FIGURE 7.   a) Correlation matrix of the cross-sectional areas of the cranial bones. b) The first two principal components (eigenvectors) of this correlation matrix (with eigenvalues 3.60 and 2.06).

Similarly, the variance of every PW, plotted against inverse BE on a log–log scale, had a regression slope of 0.65—well below 1 (Fig. 10). These results indicate a strong pattern of compensatory shape variation within the cranium. The small-scale PWs with very low variance (PW 13, 14, 19) correspond to the relative positions of the semilandmarks, which were standardized in the course of the sliding landmark algorithm and hence show little variance. PW 35, by contrast, shows considerably more

variance than expected for its spatial scale; it corresponds to the relative size and orientation of the nasal bone (Fig. 10, left).

In summary, we observed opposite patterns for variation in cranial size and shape. The cross-sectional area of cranial elements was characterized by coordinated variation and largely positive correlations among the components, whereas cranial shape showed a pattern of compensatory variation: larger cranial shape features were much less variable than smaller ones. We also identified aspects of both size and shape variation that deviated from these overall variational patterns.

---

landmark coordinates are divided by their centroid size in the course of Procrustes registration).
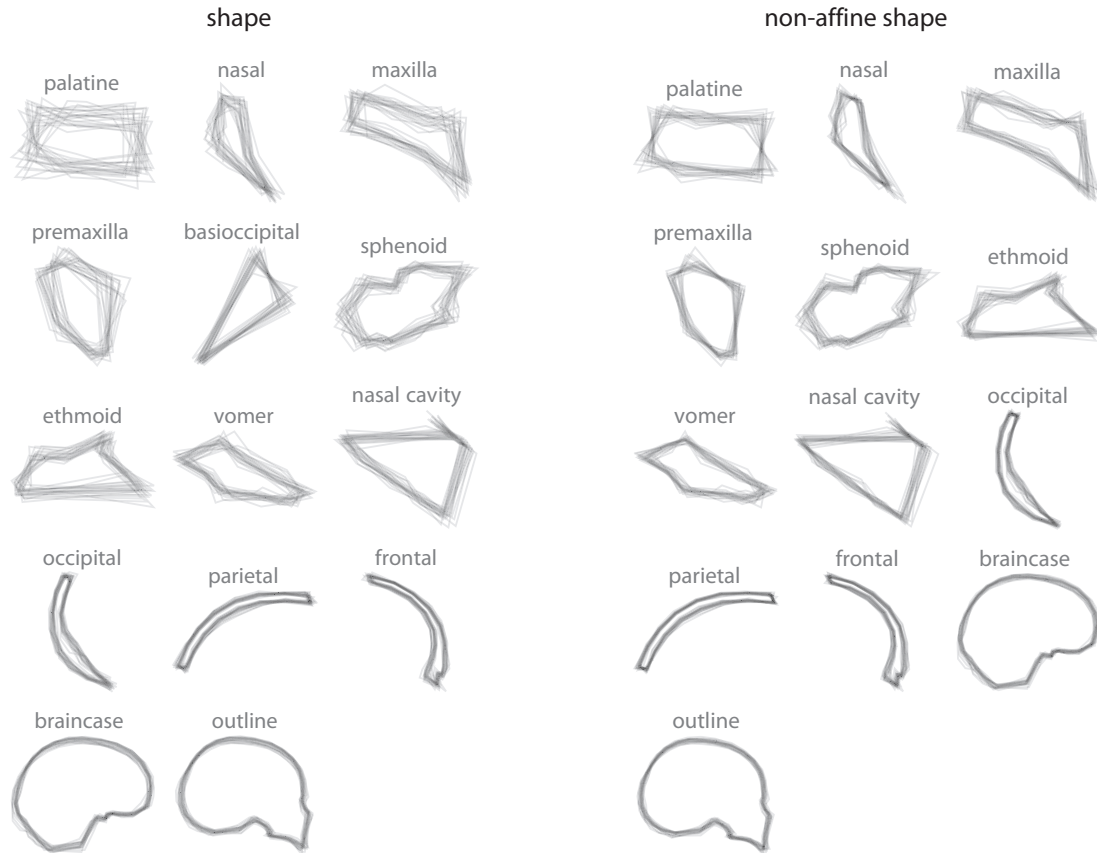
FIGURE 8.   Adult human variation in the shape of cranial bones and cavities, as delineated by the midsagittal landmarks and semilandmarks (connected into polygons). They are ordered from smallest to largest and superimposed by Generalized Procrustes Analysis (Rohlf and Slice 1990). The left panel shows the total shape variation of these cranial structures, and the right panel the nonaffine parts of shape variation. The right panel does not include the basioccipital as it was represented by three landmarks only and, hence, does not have a nonaffine component. Smaller structures vary considerably more than larger structures.
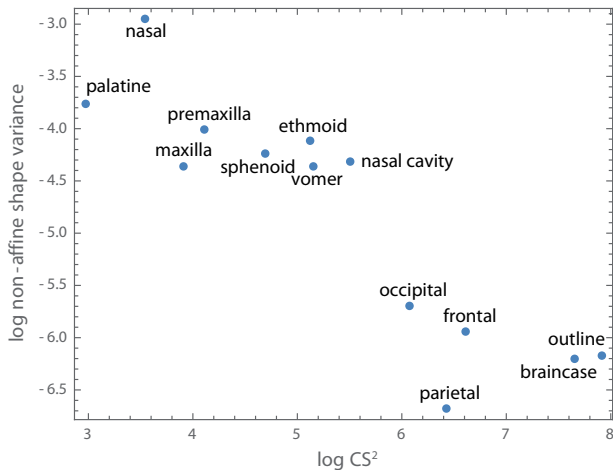

FIGURE 9.   Nonaffine shape variance versus squared average centroid size for the different cranial structures, plotted on a log–log scale.

THE (MIS)MEASURE OF SIZE AND SHAPE

Measurement error can affect the analyses described here. Independent error in size measurements biases the results towards self-similarity or nonregulation

(cf. Fig. 1), whereas independent error in landmark coordinates induces negative correlations between adjacent interlandmark distances and thus biases the results towards compensation (Figs. 4a–d and 11). Furthermore, shape variance does not become zero if the scale at which it is studied approaches zero: even very small structures show variation due to measurement error. This is referred to as "nugget effect" in geostatistics and raises the intercept of the regression of log variance on log scale. The cranial landmarks used here were measured carefully on high-resolution scans; measurement error was negligible compared to the differences in shape variance across scales (the smallest structures varied 6–25 times more than cranial outline shape). For data more prone to error, estimates of measurement error may be included in an extended regression model (Mardia et al. 2006; Bookstein 2015).

Composite measures of overall size, such as centroid size, usually are less affected by measurement error because they are computed as a (weighted) sum of many measurements; independent measurement error thus tends to average out. But while "scale" is a geometrical *a priori*, "size" involves a choice of formulas from a wide range of possibilities. The difference between the
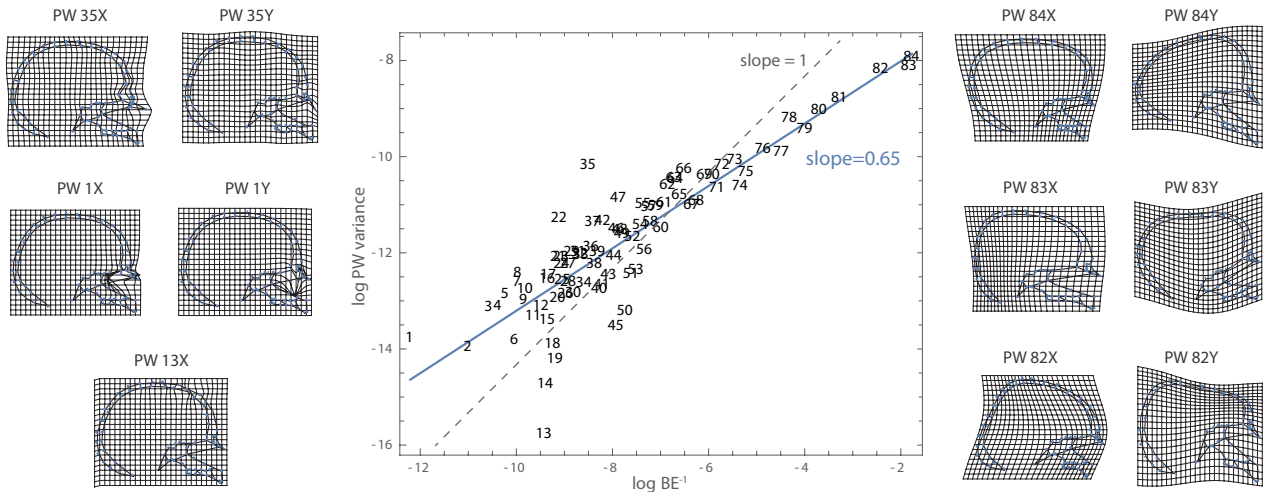
FIGURE 10.   The 87 cranial landmarks give rise to 84 PWs (with two parameters each, one for the X coordinates and one for the Y coordinates), which represent shape features of increasing spatial scale. The variance of each PW is plotted against inverse BE, as a measure of squared spatial scale (middle panel). The linear regression slope in this log–log plot is 0.65, clearly below 1. Hence, large-scale shape features (such as those visualized on the right) are less variable than expected for their scale under self-similarity; small-scale shape features (such as PW 1 shown on the left) are more variable than expected. Even relative to this scaling pattern, PW 35, the relative size and orientation of the nasal bone (top left), is hypervariable, whereas PWs 13, 14, 18, and 19 (the relative positions of semilandmarks; e.g., PW 13 on the lower left) show reduced variation.
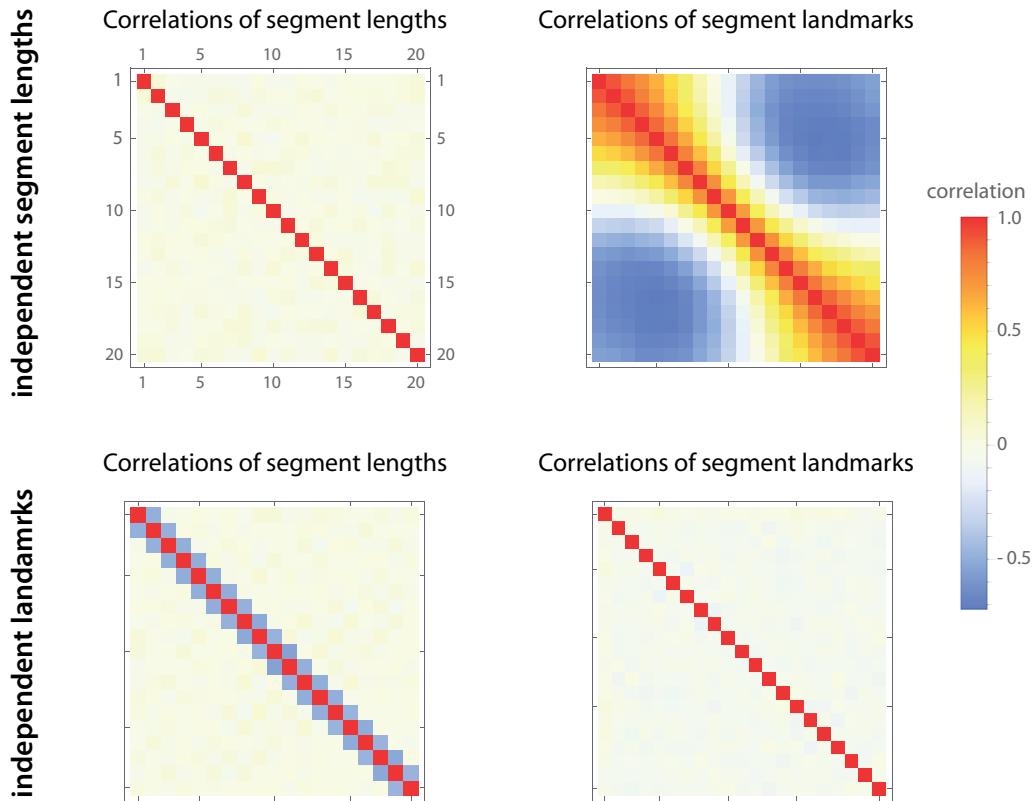

FIGURE 11.   Correlation matrices of the segment lengths (left panels) and segment borders or "landmarks" (right panels) for superimposed 1D "worms" as in Figure 1. In the upper panels, the segment lengths vary independently (like the increments in a random walk), which induces a strong pattern of spatial autocorrelation among the segment borders (the incremental steps of the random walk). In the lower panels, the positions of the segment borders vary independently (as in most null models of landmark variation), which implies negative correlations between the lengths of adjacent segments (interlandmark distances).

two choices exploited here for the cranial data, area and squared centroid size, can bear implications for the biological inferences that ensue (Mitteroecker et al. 2013; Bookstein 2018). For the present data, however, these two measures led to very similar results.

Our approach does not apply to standardized size measures, such as measures scaled to the same sum in each individual. The ensuing *relative* dimensions necessarily exhibit negative correlations and reduced (or zero) variation at large scale, but this cannot be biologically interpreted. Similarly, Procrustes superimposition standardizes overall location, orientation, and scale in a sample of landmark configurations (Rohlf and Slice 1990). As a result, the relative size of a contiguous subset of landmarks is negatively correlated with the relative size of the remaining landmarks. For example, after Procrustes superimposition, a small face necessarily coincides with a large neurocranium. Hence, our approach to study coordination and compensation of shape is not based on the comparison of relative sizes but on the comparison of nonaffine shape variation at different scales.

Discussion

Morphological Integration

Phenotypic correlations among traits are usually discussed in the context of morphological integration (e.g., Olson and Miller 1958; Cheverud 1982; Mitteroecker and Bookstein 2007; Klingenberg and Marugan-Lobon 2013; Armbruster et al. 2014; Klingenberg 2014; Billet and Bardin 2019), which has two historical and conceptual origins. In evolutionary quantitative genetics, correlations among traits are estimated for modeling indirect evolutionary responses to selective pressures, but they are rarely interpreted in a developmental contexts (Fisher 1930; Lande 1979; Roff 1997). By contrast, in early factor analysis and path modeling, as developed by Sewall Wright, Paul Terentjev, and others (Terentjev 1931; Wright 1932, 1934), the correlation structure of a set of morphometric variables was explicitly modeled for inferring the growth factors that shaped the organism. But Wright and Terentjev were studying mainly size measures of distinct anatomical elements (e.g., long bones). With Olson and Miller's influential 1958 book, these traditions were fused in an unfortunate manner: raw correlations were interpreted in both the evolutionary and developmental context, with a correlation of zero as benchmark for evolutionary as well as developmental independence (but see, e.g., Cheverud 1984; Gromko 1995). With the advent of modern measurement and imaging technologies, the same rationale was applied to larger collections of linear distances within complex structures, such as the cranium, and even to the shape coordinates of landmarks. But for such landmarks or interlandmark distances, a null model of all correlations zero is difficult to reify biologically.

Consider, for instance, the self-similar "worms" in Figure 1, where the lengths of the 20 segments are all mutually uncorrelated: nonintegrated variation of segment lengths. But the 21 landmarks separating these segments, superimposed by mean-centering the coordinates of every specimen, show a strong spatial auto-correlation (Fig. 11, upper panels): adjacent landmarks are positively correlated, even though the distances between them are not. Only more distant landmarks are uncorrelated or even negatively correlated (due to the superimposition). Such a pattern of spatial autocorrelation is very common for morphometric data (Mitteroecker and Bookstein 2007; Gonzalez et al. 2019). Even though consistent with a model of completely unintegrated development, it can explain the results in many published studies on variational modularity (Mitteroecker 2009). In "worms" with completely uncorrelated landmark positions (i.e., uncorrelated segment borders, not segment lengths), the lengths of adjacent segments are necessarily negatively correlated (Fig. 11, lower panels). But an interpretation of these negative correlations among adjacent elements in terms of compensatory processes would be misleading.

For a biological interpretation of phenotypic correlations it is thus important to consider the level at which developmental regulation occurs, at the landmark locations or in the spaces in-between. Often it may be the latter or a combination of both. For this reason, a self-similar landmark distribution can be a more useful reference distribution than a distribution of independent and identically distributed variation at every landmark (Bookstein 2015, 2017).

Developmental Origins and Evolutionary Relevance of Coordination and Compensation

Positive correlations among the sizes of anatomical elements—which we found to be prevalent within the human cranium—have also been reported in many previous studies. Coordinated growth can result from shared developmental timing and growth rates, similar gene expression patterns, and growth factors with systemic effects (e.g., growth hormones; Hallgrimsson et al. 2007a,b; Mitteroecker et al. 2012; Hall 2015). Well-documented genes with coordinated (pleiotropic) effects on growth at cranial sutures of dermal bones and synchondroses in the cranial base include *HGH* and members of the *BMP*, *TGF*-β, and *FGF* gene families (Opperman 2000; Hall 2015).

Whereas condensation and early growth rates of bone and cartilage are mainly controlled independent of extracellular influences, later cranial growth is coordinated by multiple stimuli from adjacent tissues (Moss and Young 1960; Herring 1993; Hallgrimsson et al. 2007a; Lieberman 2011). For instance, brain size largely coordinates the size of the encapsulating neurocranium, and the dura mater plays an important signaling role in keeping the sutures of the overlying flat bones unfused and patent (Opperman et al. 1996; Moss 1997;

Mitteroecker and Bookstein 2008; Bastir et al. 2010; Lieberman 2011). Coordinating effects of brain size on cranial form are most obvious in cases of hydrocephaly or microcephaly (Young 1959; Huggare et al. 1989). Similarly, dental occlusion as well as forces exerted during mastication and by the tongue are important factors that coordinate postnatal facial growth (Enlow and Hans 1996; Moss 1997).

The genetic and developmental origins of compensatory variation—which we found to dominate cranial shape—are less well known. Growth factors with opposite effects on different tissues and cell apoptosis induced by adjacent cells are documented for embryonic development, but they are unlikely to account for the compensatory growth patterns in fetal and postnatal cranial growth. One mechanism underlying compensatory variation in the cranium may be mechanically induced bone growth. Bone is susceptible to mechanical forces acting on it and adapts to the stresses it is exposed to. Through mechanotransduction, local mechanical loading induces a signaling cascade from mechanosensory cells (osteocytes) to osteoblasts (bone-synthesizing cells), initiating the formation of bony matrix until the strain is normalized. When mechanical loading is reduced, osteoclasts are signaled to break down bone ("bone mechanostat"; Huiskes et al. 2000; Frost 2003; Skerry and Suva 2003; Watson et al. 2018). Bone formation and remodeling in response to mechanical forces are also documented for the cranium. For instance, tooth movement during dental development or orthodontic treatment occurs through bone resorption at sites of bone compression and bone formation at sites of tension (Enlow and Hans 1996; Zhong et al. 2013; Wang et al. 2018). Mechanical forces also influence bone growth at sutures and synchondroses, even though the actual mechanisms are complex and differ between static and cyclical load. However, both animal experiments and human treatment with orthodontic appliances suggest that suture growth is promoted by tension and retarded by compression (Parr et al. 1997; Sun et al. 2004; Koudstaal et al. 2005; Herring 2008).

We propose that mechanically induced bone formation and remodeling are the main mechanisms underlying compensatory bone growth in the developing cranium: excessive growth of a bone exerts pressure on adjacent bones, which react by osteoclast activity and bone resorption. Conversely, reduced growth of a cranial bone exerts tension and increases osteoblast activity in the neighboring bones. As a result, cranial bones grow by compensating excessive or stunted growth in their environment. Evidence for such compensatory growth comes from craniosynostosis, the premature closure of cranial sutures. Because growth perpendicular to the fused suture is restricted, compensatory growth occurs parallel to the fused suture, primarily in the adjacent bones (Delashaw et al. 1989; Flaherty et al. 2016).

Clearly, these developmental mechanisms cannot be inferred from morphometric data alone. But the relative extents of genetically determined versus mechanically induced compensatory bone growth can be studied by contrasting compensatory shape variation among twins and among unrelated individuals, or in lab species, among isogenic individuals and within natural populations. Genetically determined compensatory variation would be greatly reduced among twins and in isogenic samples, whereas mechanically induced compensatory variation would be less affected by genetic heterogeneity. If compensatory growth is indeed largely mechanically induced, not genetically, then one would further expect that *within a population* the heritability of cranial shape is higher for large scale features than for small scale features and also higher for coordinated variation than for compensatory variation. Compensatory variation *between populations*, however, also would have some genetic basis and, because of its reduced functional importance, is expected to show a stronger phylogenetic signal than coordinated variation and large-scale features.

Compensatory growth appears essential for buffering developmental, environmental, and also genetic perturbations, thus enabling a stable, canalized development (Debat and David 2001; Siegal and Bergman 2002; Zelditch et al. 2006; Mitteroecker et al. 2012). But developmental mechanisms of compensation and coordination may also be prerequisites of an integrated evolutionary change of composite structures, such as the cranium or pelvis, and constitute a key component of their "evolvability" (Kirschner and Gerhart 1998; Hendrikse et al. 2007). Such anatomical structures typically show a complex genetic architecture, involving numerous genes with overlapping and partly opposing pleiotropic effects (Pavlicev and Wagner 2012). Appropriate genetic response to directional selection therefore necessitates a joint allelic change at multiple loci, which may be impeded by recombination, especially when involving new mutations. Early responses to selection thus require the "epigenetic," mechanically induced integration of anatomical elements in order to preserve spatial and functional integrity. These epigenetic processes during development may later be fixed by genetic assimilation or remain part of the evolved developmental program.

References

Armbruster W.S., Pélabon C., Bolstad G.H., Hansen T.F. 2014. Integrated phenotypes: understanding trait covariation in plants and animals. Philos. Trans. R. Soc. Lond. B Biol. Sci. 369:20130245.

Bartsch S. 2019. The ontogeny of hominid cranial form: a geometric morphometric analysis of coordinated and compensatory processes [Master's Thesis]. University of Vienna.

Bastir M., Rosas A., Stringer C., Manuel Cuétara J., Kruszynski R., Weber G., Ross C., Ravosa M. 2010. Effects of brain and facial size on basicranial form in human and primate evolution. J. Hum. Evol. 58:424–431.

Billet G., Bardin J. 2019. Serial homology and correlated characters in morphological phylogenetics: modeling the evolution of dental crests in placentals. Syst. Biol. 68:267–280.

Bookstein F. 1991. Morphometric tools for landmark data: geometry and biology. Cambridge (UK): Cambridge University Press.

Bookstein F. 1997. Landmark methods for forms without landmarks: morphometrics of group differences in outline shape. Med. Image Anal. 1:225–243.

Bookstein F.L. 1989. Principal warps: thin plate splines and the decomposition of deformations. IEEE Trans. Patt. Anal. Mach. Intell. 11:567–585.

Bookstein F.L. 2015. Integration, disintegration, and self-similarity: characterizing the scales of shape variation in landmark data. Evol. Biol. 42:395–426.

Bookstein F.L. 2017. A method of factor analysis for shape coordinates. Am. J. Phys. Anthropol. 164:221–245.

Bookstein F.L. 2018. A course in morphometrics for biologists: geometry and statistics for studies of organismal form. Cambridge, UK: Cambridge University Press.

Cannon M.J., Percival D.B., Caccia D.C., Raymond G.M., Bassingthwaighte J.B. 1997. Evaluating scaled windowed variance methods for estimating the Hurst coefficient of time series. Physica A 241:606–626.

Cheverud J. 1982. Phenotypic, genetic, and environmental morphological integration in the cranium. Evolution 36:499–516.

Cheverud J. 1984. Quantitative genetic and developmental constraints on evolution by selection. J. Theor. Biol. 110:155–171.

Debat V., David P. 2001. Mapping phenotypes: canalization, plasticity and developmental stability. Trends Ecol. Evol. 16:555–561.

Delashaw J.B., Persing J.A., Broaddus W.C., Jane J.A. 1989. Cranial vault growth in craniosynostosis. J. Neurosurg. 70:159–165.

Embrechts P., Maejima M. 2002. Selfsimilar processes. Princeton, NJ: Princeton University Press.

Enlow D., Hans, M. 1996. Essentials of facial growth. Philadelphia, PA: Saunders Company.

Fisher R.A. 1930. The genetical theory of natural selection. Oxford, UK: Clarendon.

Flaherty K., Singh N., Richtsmeier J.T. 2016. Understanding craniosynostosis as a growth disorder. Wiley Interdiscip. Rev. Dev. Biol. 5:429–459.

Frost H.M. 2003. Bone's mechanostat: a 2003 update. Anat. Rec. A Discov. Mol. Cell Evol. Biol. 275:1081–1101.

Gerard R.W. editor. 1958. Concepts of biology. Publication 560. National Academy of Sciences, National Research Council.

Gonzalez P.N., Bonfili N., Vallejo Azar M.N., Barbeito-Andres J., Bernal V., Perez S. I. 2019. Description and analysis of spatial patterns in geometric morphometric data. Evol. Biol. 46:260–270.

Gray H. 1918. Anatomy of the Human Body. Philadelphia, PA: Lea & Febiger.

Gromko M.H. 1995. Unpredictability of correlated response to selection: pleiotropy and sampling interact. Evolution 49:685–693.

Gunz P., Mitteroecker, P. 2013. Semilandmarks: a method for quantifying curves and surfaces. Hystrix 24:103–109.

Hall B.K. 2015. Bones and cartilage: developmental skeletal biology. 2nd ed. Amsterdam: Academic Press.

Hallgrímsson B., Katz D., Aponte J.D., Larson J.R., Devine J., Gonzalez P., Young N.M., Roseman C.C., Marcucio R.S. 2019. Integration and the developmental genetics of allometry. Integr. Comp. Biol. 59:1369–1381.

Hallgrimsson B., Lieberman D.E., Liu W., Ford-Hutchinson A.F., Jirik F.R. 2007a. Epigenetic interactions and the structure of phenotypic variation in the cranium. Evol. & Dev. 9:76–91.

Hallgrimsson B., Lieberman D.E., Young N.M., Parsons T., Wat S. 2007b. Evolution of covariance in the mammalian skull. Novartis Found. Symp. 284:164–190.

Hendrikse J.L., Parsons T.E., Hallgrímsson B. 2007. Evolvability as the proper focus of evolutionary developmental biology. Evol. Dev. 9:393–401.

Herring S.W. 1993. Epigenetic and functional influences on skull growth. In: Hanken J., Hall B., editors. The skull, vol. 1. Chicago: The University of Chicago Press. p. 153–206.

Herring S.W. 2008. Mechanical influences on suture development and patency. Front. Oral Biol. 12:41–56.

Hodin J. 2000. Plasticity and constraints in development and evolution. J. Exp. Zool. 288:1–20.

Huggare J., Kantomaa T., Serlo W., Rönning O. 1989. Craniofacial morphology in untreated shunt-treated hydrocephalic children. Acta Neurochir. (Wien) 97:107–110.

Huiskes R., Ruimerman R., van Lenthe G.H., Janssen J.D. 2000. Effects of mechanical forces on maintenance and adaptation of form in trabecular bone. Nature 405:704–706.

Hurst H.E. 1951. Long-term storage capacity of reservoirs. Trans. Am. Soc. Civil Eng. 116:770–799.

Kent J.T., Mardia K.V. 1994. The link between kriging and thin-plate splines. In: Kelly F.P., editor. Probability, statistics and optimization: a tribute to Peter Whittle. Chichester: Wiley. p. 325–339.

Kirschner M., Gerhart J. 1998. Evolvability. Proc. Natl. Acad. Sci. USA 95:8420–8427.

Klingenberg C.P. 2014. Studying morphological integration and modularity at multiple levels: concepts and analysis. Philos. Trans. R. Soc. Lond. B Biol. Sci. 369:20130249.

Klingenberg C.P., Marugan-Lobon J. 2013. Evolutionary covariation in geometric morphometric data: analyzing integration, modularity, and allometry in a phylogenetic context. Syst. Biol. 62:591–610.

Koudstaal M.J., Poort L.J., van der Wal K. G.H., Wolvius E.B., Prahl-Andersen B., and Schulten A. J.M. 2005. Surgically assisted rapid maxillary expansion (SARME): a review of the literature. Int. J. Oral Maxillofac. Surg. 34:709–714.

Lande R. 1979. Quantitative genetic analysis of multivariate evolution, applied to brain:body size allometry. Evolution 33:402–416.

Leland W.E., Taqqu M.S., Willinger W., Wilson D.V. 1994. On the self-similar nature of ethernet traffic. IEEE/ACM Trans. Netw. 2: 1–15.

Lieberman D.E. 2011. The evolution of the human head. Cambridge, MA: Belknap Press/Harvard University Press.

Mandelbrot B.B., Van Ness J.W. 1968. Fractional Brownian motions, fractional noises and applications. SIAM Rev. 10:422–437.

Mardia K.V., Bookstin F.L., Kent J.T., Meyer C.R. 2006. Intrinsic random fields and image deformations. J. Math. Imaging Vis. 26: 59–71.

Mitteroecker P. 2009. The developmental basis of variational modularity: insights from quantitative genetics, morphometrics, and developmental biology. Evol. Biol. 36:377–385.

Mitteroecker P., Bookstein F.L. 2007. The conceptual and statistical relationship between modularity and morphological integration. Syst. Biol. 56:818–836.

Mitteroecker P., Bookstein F.L. 2008. The evolutionary role of modularity and integration in the hominoid cranium. Evolution 62:943–958.

Mitteroecker P., Gunz P., Neubauer S., Muller G. 2012. How to explore morphological integration in human evolution and development? Evol. Biol. 39:536–553.

Mitteroecker P., Gunz P., Windhager S., Schaefer, K. 2013. Shape, form, and allometry in geometric morphometrics, with applications to human facial morphology. Hystrix 24:59–66.

Moss M., Young, R. 1960. A functional approach to craniology. Am. J. Phys. Anthropol. 18:281–292.

Moss M.L. 1997. The functional matrix hypothesis revisited. 4. The epigenetic antithesis and the resolving synthesis. Am. J. Orthod. Dentofacial Orthop., 112:410–417.

Olson E.C., Miller R.L. 1958. Morphological integration. Chicago: University of Chicago Press.

Opperman L., Passarelli R., Nolen A., Gampper T., Lin K., Ogle R. 1996. Dura mater secretes soluble heparin-binding factors required for cranial suture morphogenesis. In Vitro Cell Dev. Biol. 32: 627–632.

Opperman L.A. 2000. Cranial sutures as intramembranous bone growth sites. Dev. Dyn. 219:472–485.

Parr J.A., Garetto L.P., Wohlford M.E., Arbuckle G.R., Roberts W.E. 1997. Sutural expansion using rigidly integrated endosseous implants: an experimental study in rabbits. Angle Orthod. 67:283–290.

Pavlicev M., Wagner G.P. 2012. A model of developmental evolution: selection, pleiotropy and compensation. Trends Ecol. Evol. 27:316–322.

R Core Team. 2019. R: a language and environment for statistical computing. Vienna (Austria): R Foundation for Statistical Computing. Available from: https://www.R-project.org/.

Roff D.A. 1997. Evolutionary quantitative genetics. New York: Chapman & Hall.

Rohlf F., Bookstein F.L. 2003. Computing the uniform component of shape variation. Syst. Biol. 52:66–69.

Rohlf F.J., Slice D.E. 1990. Extensions of the procrustes method for the optimal superimposition of landmarks. Syst. Zool. 39: 40–59.

Siegal M.L., Bergman A. 2002. Waddington's canalization revisited: developmental stability and evolution. Proc. Natl. Acad. Sci. USA 99:10528–10532.

Skerry T.M., Suva L.J. 2003. Investigation of the regulation of bone mass by mechanical loading: from quantitative cytochemistry to gene array. Cell Biochem. Funct. 21:223–229.

Sun Z., Lee E., Herring S.W. 2004. Cranial sutures and bones: growth and fusion in relation to masticatory strain. Anat. Rec. A Discov. Mol. Cell Evol. Biol. 276:150–161.

Terentjev P. 1931. Biometrische untersuchungen über die morphologischen merkmale von rana ridibunda pall (amphibia, salientia). Biometrika 23:23–51.

Wake D.B. 1991. Homoplasy: the result of natural selection, or evidence of design limitations? Am. Nat. 138:543–567.

Wang Y., Jia L., Zheng Y., Li W. 2018. Bone remodeling induced by mechanical forces is regulated by miRNAs. Biosci. Rep. 38:BSR20180448.

Watson P.J., Fitton L.C., Meloro C., Fagan M.J., Gröning F. 2018. Mechanical adaptation of trabecular bone morphology in the mammalian mandible. Sci. Rep. 8:7277.

Wright S. 1932. General, group and special size factors. Genetics 15:603–619.

Wright S. 1934. The method of path coefficients. Ann. Math. Stat. 6:161–215.

Young R.W. 1959. The influence of cranial contents on postnatal growth of the skull in the rat. Am. J. Anat. 105:383–415.

Zelditch M.L., Mezey J.G., Sheets H.D., Lundrigan B.L., Garland T. 2006. Developmental regulation of skull morphology II: ontogenetic dynamics of covariance. Evol. Dev. 8:46–60.

Zhong Z., Zeng X.-L., Ni J.-H., Huang X.-F. 2013. Comparison of the biological response of osteoblasts after tension and compression. Eur. J. Orthod. 35:59–65.